Journal of Solid State Chemistry **159,** 371–378 (2001)
doi:10.1006/jssc.2001.9167, available online at http://www.idealibrary.com on IDEAL®

Topological Control in Two-Dimensional Cobalt(II) Coordination Polymers by π–π Stacking Interactions: Synthesis, Spectroscopic Characterization, Crystal Structure, and Magnetic Properties

Giannis S. Papaefstathiou and Spyros P. Perlepes[1]

Department of Chemistry, University of Patras, 26500 Patras, Greece
E-mail: perlepes@patreas.upatras.gr

Albert Escuer[1] and Ramon Vicente

Departament de Química Inorgànica, Universitat de Barcelona, Av. Diagonal 647, 08028 Barcelona, Spain
E-mail: albert.escuer@antares.qi.ub.es

Anastasios Gantis, Catherine P. Raptopoulou, Alexandros Tsohos, Vassilis Psycharis,[1] and Aris Terzis

Institute of Materials Science, NCSR "Demokritos", 15310 Aghia Paraskevi Attikis, Greece
E-mail: vpsychar@ims.demokritos.gr

and

Evangelos G. Bakalbassis

Department of Chemistry, Aristotle University of Thessaloniki, 54006 Thessaloniki, Greece

Received March 20, 2001; accepted March 21, 2001

IN DEDICATION TO THE LATE PROFESSOR OLIVIER KHAN FOR HIS PIONEERING CONTRIBUTIONS TO THE FIELD OF MOLECULAR MAGNETISM

The reactions of CoX_2 (X = Br, Cl) with the planar, bidentate bridging ligand 2,1,3-benzothiadiazole (btd) in Me_2CO led to the 2D coordination polymers $\{[CoBr_2(btd)]\}_n$ (1) and $\{[CoCl_2(btd)]\}_n$ (2). The structure of 1 was determined by single-crystal X-ray crystallography. Complex 1 ($C_6H_4Br_2CoN_2S$, monoclinic, $P2_1/m$, $a = 3.742(3)$, $b = 13.075(9)$, $c = 9.092(6)$ Å, $\beta = 90.09(2)^\circ$, $Z = 2$, θ–2θ, $R_1 = 0.0298$, w$R_2 = 0.0793$) consists of $\{[Co(\mu\text{-}Br)_2]\}_n$ linear chains running along the *a* axis linked via μ-btd ligands along the *b* axis. The columns of stacked btd molecules present in the crystal structure of the free ligand are maintained in the lattice of 1. XRD data revealed that 2 is isostructural with 1. The magnetic properties of both complexes can be explained by the presence of a very weak ferromagnetic intrachain Co ⋯ Co exchange interaction through the $(\mu\text{-}X)_2$ bridges and a moderate antiferromagnetic Co ⋯ Co interaction through the μ-btd bridges. The new complexes were also characterized by EPR, IR, and UV/VIS spectra, and all data are discussed in terms of the nature of bonding and known structures.

Key Words: **aromatic stacking interactions; 2,1,3-benzothiadiazole; cobalt(II); coordination polymers; crystal engineering; magnetic properties of 2D systems; Rietveld analysis; single-crystal X-ray crystallography.**

[1] To whom correspondence should be addressed.

INTRODUCTION

Crystal engineering and the design of solid-state architectures has become an area of increasing interest over recent years (1–3). Among a plethora of supramolecular assemblies, self-assembled coordination polymers are newer members of this family. The most common strategy that has thus far been applied in the context of the design of coordination polymers is to generate a coordination polymeric network by the extension of the metal's coordination geometry employing exodentate bifunctional ligands to link the metal ions (4). The structure and the properties of the resulting polymer strongly depend on the coordination preferences of the metal ion and the coordination ability of the bridging ligand (5). These two factors are not the only ones that should be taken into account in order to construct a coordination polymer. There is also a combination of other weaker, noncovalent interactions, such as hydrogen

0022-4596/01 $35.00

bonding and van der Waals forces, which, often, influence the self-assembly process (6–8).

Interactions between aromatic molecules represent an important class of nondirectional forces in chemistry, biology, and materials science (9, 10). They control a variety of molecular recognition and self-assembly phenomena, including the packing of aromatic molecules (and therefore the materials properties of these compounds) and template-directed synthesis. Hence, their significance in crystal engineering should not be underestimated.

An example of the role of stacking interactions is provided by the structure of the potentially bidentate bridging ligand 2,1,3-benzothiadiazole (btd), which consists (11) of columns of stacked molecules (intermolecular distance 3.50 Å) running along one of the crystallographic axes; there is no significant interaction between adjacent columns. The btd molecule has a fixed bridging angle and its coordination chemistry has rather been neglected (12–15). If the free ligand reacts with suitable metal-containing starting materials, such as cobalt(II) bromide or chloride, an additional structure-determining factor is introduced, namely the coordination bond, leading to the construction of the two-dimensional (2D) coordination polymers, $\{[CoBr_2(btd)]\}_n$ and $\{[CoCl_2(btd)]\}_n$. These polymers are the subject of this paper.

From the magnetic point of view the ideal 2D Heisenberg spin systems are theoretically predicted not to show magnetic ordering at any finite temperature, but real 2D materials show various magnetic transitions (16). Despite the fact that the ground states and the transition temperatures of the 2D layered systems are usually governed by the *intra*layer interactions, weak *inter*layer interactions and magnetic anisotropy can influence the bulk properties of these materials. In particular, Co^{II}-layered materials have been shown to exhibit long-range magnetic order (17), ferrimagnetic or metamagnetic behavior (18–20), and canted antiferromagnetism (21).

Furthermore coordination polymers exhibiting layered structures could be used to create magnetic multilayered phases. These materials are crystalline and therefore have a higher degree of perfection than magnetic multilayers obtained by deposition techniques and other physical methods (22).

We will show here how the aromatic stacking interactions are able to create a structural frame strong enough to determine the dimensionality and the nature of the resulting network. The magnetic properties of the two 2D polymers show that both complexes are governed by antiferomagnetic coupling between very weak ferromagnetic chains.

EXPERIMENTAL

General Considerations

All manipulations were performed under aerobic conditions. All chemicals were purchased from commercial sources and used without further purification. C, H, and N microanalyses were conducted by the microanalytical service of the University of Ioannina, Greece. IR spectra (4000–450 cm^{-1}) were recorded as KBr pellets on a Perkin–Elmer 16PC FTIR spectrometer. Solid-state (diffuse reflectance, 28.5–12.5 kK) electronic spectra were recorded on a Varian Cary 100 instrument. Magnetic susceptibility measurements were carried out for polycrystalline samples of the complexes in the range 2.0–300 K under various magnetic fields by using a SQUID susceptometer. The experimental magnetic susceptibilities were corrected for the diamagnetic response using Pascal's constants. Solid-state EPR spectra were recorded on a Bruker ES200 spectrometer at X-band frequency. X-ray powder diffraction data (XRD) were recorded on a Siemens D500 diffractometer employing Cu$K\alpha$ radiation ($\lambda = 1.5418$ Å) and a secondary beam graphite monochromator. The measured 2θ range (2°–80°) was scanned in steps of 0.03° with a counting time of 6 s per step. The aperture and soller slits were set at 1.0°.

Synthesis

$\{[CoBr_2(btd)]\}_n$ (**1**). To a dark blue solution of $CoBr_2$ (0.25 g, 1.14 mmol) in Me_2CO (10 mL) was added under stirring a colorless solution of btd (0.15 g, 1.10 mmol) in the same solvent (5 mL). A green microcrystalline powder of **1** appeared within 5 min.; this was filtered, washed with Me_2CO, and dried over $CaCl_2$. Yield: 0.27 g (70%). Anal. Calcd for $C_6H_4Br_2CoN_2S$: C, 20.30%; H, 1.13%; N, 7.89%. Found: C, 20.20%; H, 1.20%; N, 7.81%. X-ray quality single crystals of **1** were obtained by layering of an Me_2CO solution (10 mL) of $CoBr_2$ (0.25 g, 1.14 mmol) over a $CHCl_3$ solution (15 mL) of btd (0.15 g, 1.10 mmol). Slow mixing yielded green crystals of **1** within 2–3 days. Yield: 0.20 g (50%). Selected IR data (cm^{-1}): 1532 (s), 1480 (s), 1434 (s), 924 (s), 870 (vs), 848 (s), 734 (vs), 592 (m).

$\{[CoCl_2(btd)]\}_n$ (**2**). To a royal blue solution of $CoCl_2$ (0.15 g, 1.15 mmol) in Me_2CO (10 mL) was added under stirring a colorless solution of btd (0.15 g, 1.10 mmol) in the same solvent (5 mL). A green microcrystalline powder of **2** appeared immediately; this was filtered, washed with Me_2CO, and dried over $CaCl_2$. Yield: 0.23 g (80%). Anal. Calcd for $C_6H_4Cl_2CoN_2S$: C, 27.09%; H, 1.51%; N, 10.53%. Found: C, 26.99%; H, 1.45%; N, 10.61%. Selected IR data (cm^{-1}): 1534 (m), 1484 (m), 1436 (m), 926 (m), 874 (s), 854 (m), 736 (vs), 594 (m).

Single-Crystal X-Ray Structure Determination

A prismatic crystal of **1** was mounted in air. Diffraction measurements were made on a Crystal Logic Dual Goniometer diffractometer using graphite-monochromated Mo radiation. Unit cell dimensions were determined and refined by using the angular settings of 25 automatically

TABLE 1
Crystal Data, Data Collection, and Structure Refinement Details for $\{[CoBr_2(btd)]\}_n$ (1)

Empirical formula	$C_6H_4Br_2CoN_2S$
Formula weight	354.92
Temperature (K)	298
λ(Mo$K\alpha$) (Å)	0.71073
Crystal size (mm)	$0.15 \times 0.30 \times 0.50$
Crystal system	Monoclinic
Space group	$P2_1/m$
a (Å)	3.742(3)
b (Å)	13.075(9)
c (Å)	9.092(6)
β (°)	90.09(2)
V (Å^3)	444.9(5)
Z	2
ρ_{calc} (g cm^{-3})	2.649
μ (mm^{-1})	11.0082
Transition factors (T_{min}/T_{max})	0.51/1.00
Scan mode/speed (° min^{-1})	θ–2θ/4.0
Scan range (°)	$2.5 + a_1a_2$ separation
θ range (°)	2.24 to 25.99
h	0 to 4
k	−16 to 16
l	−11 to 11
F (000)	334
Reflections collected	2016
Unique reflections (R_{int})	914 (0.0338)
Data with $I > 2\sigma(I)$	885
Parameters refined	67
$[\Delta/\sigma]_{max}$	0.084
$(\Delta p)_{max}$, $(\Delta p)_{min}$ (e Å^{-3})	0.552, −0.713
w^a	$a = 0.0416$, $b = 0.3901$
GoF (on F^2)	1.203
$R_1{}^b$ $[I > 2\sigma(I)]$	0.0298
$R_2{}^c$ $[I > 2\sigma(I)]$	0.0793

[a] $w = 1/[\sigma^2(F_o^2) + (aP)^2 + bP]$ and $P = (\max(F_o^2, 0) + 2F_c^2)/3$.
[b] $R_1 = \sum(|F_o| - |F_c|)/\sum(|F_o|)$.
[c] $wR_2 = \{\sum[w(F_o^2 - F_c^2)^2]/\sum[w(F_o^2)^2]\}^{1/2}$.

centered reflections in the $11^\circ < 2\theta < 23^\circ$ range. Three standard reflections monitored every 97 reflections showed less than 3% variation and no decay. Lorentz, polarization, and Ψ-scan absorption corrections were applied using Crystal Logic software. The structure was solved by direct methods using SHELXS-86 (23) and refined by full-matrix least-squares techniques on F^2 with SHELXL-93 (24). All hydrogen atoms were located by difference maps and refined isotropically. All nonhydrogen atoms were refined anisotropically. Crystal data, details of data collection, and structure refinement are tabulated in Table 1. Atomic coordinates of **1** are listed in Table 2.

RESULTS AND DISCUSSION

Syntheses and Structures

Reaction of btd with an equivalent of $CoBr_2$ in Me_2CO gives a blue-green solution from which $\{[CoBr_2(btd)]\}_n$ **1** precipitates within 3–4 min. in approx. 70% yield. Layering of an Me_2CO solution of $CoBr_2$ over a $CHCl_3$ solution of btd (in a 1:1 molar ratio) gives green crystals of **1** in approx. 50% total yield. Complex **1** can also be isolated by employing $CoBr_2$: btd molar ratios of 2:1, 1:2, 1:3, 1:4, 1:5, and 1:6 in a variety of organic solvents like Me_2CO, MeCN, EtOH, Pr^{n}OH, and THF, as well as in several mixtures of these solvents.

TABLE 2
Positional ($\times 10^4$) and Equivalent Thermal Parameters ($\times 10^3$) of the Nonhydrogen Atoms for Complex 1

Atom	x	y	z	U_{eq} (Å^2)[a]
Co	5000	5000	0	21
Br	− 1(1)	4431(1)	1795(1)	24
N1	5013(8)	3445(2)	−949(3)	25
S	4998(4)	2500	207(1)	30
C6	5007(11)	3045(3)	− 4933(4)	39
C7	5009(12)	3596(3)	− 3680(5)	34
C9	5008(9)	3048(3)	− 2330(4)	24

[a] U_{eq} is defined as one-third of the trace of the orthogonalized U_{ij} tensor.

Selected bond distances and angles for compound **1** are listed in Table 3. The solid consists of 1D $\{Co(\mu\text{-}Br)_2\}_n$ linear chains running along the a axis linked via μ-btd ligands along the b axis to afford an extended 2D layered network (Fig. 1), with intranetwork Co ⋯Co separations of 3.742(3) (via bromides) and 6.538(1) Å (via btd). The shortest internetwork Co ⋯Co separation is 9.092 Å. The Co^{II} atom sits on an inversion center while a mirror plane, perpendicular to the btd plane, passes through S. Each Co^{II} atom is octahedrally coordinated to four Br^- ligands and two btd molecules. The Co–Br distances are 2.590(1) and 2.594(1) Å and the Co–N bond length is 2.208(3) Å. Complex **1** has a similar structure with $[CuCl_2(pyz)]_n$ (pyz = pyrazine) (25).

A characteristic structural feature common to free btd and **1** is the existence of strong face-to-face intralayer stacking interactions between the btd ligands along the a axis (Fig. 2). The btd molecules form columns within the crystal

TABLE 3
Selected Bond Distances (Å) and Angles (°) for 1

Co–N1	2.208(3)	Br–Co–Br[b]	180.0
Co–Br	2.594(1)	N1[b]–Co–Br	90.9(1)
Co–Br[a]	2.590(1)	Br[a]–Co–Br[b]	87.6(1)
		Br[a]–Co–Br[c]	180.0
N1–Co–N1[b]	180.0	S–N1–Co	116.6(2)
N1–Co–Br[a]	88.8(1)		

Note. Symmetry transformations are used to generate equivalent atoms.
[a] $x + 1, y, z$.
[b] $-x + 1, -y + 1, -z$.
[c] $-x, -y + 1, -z$.

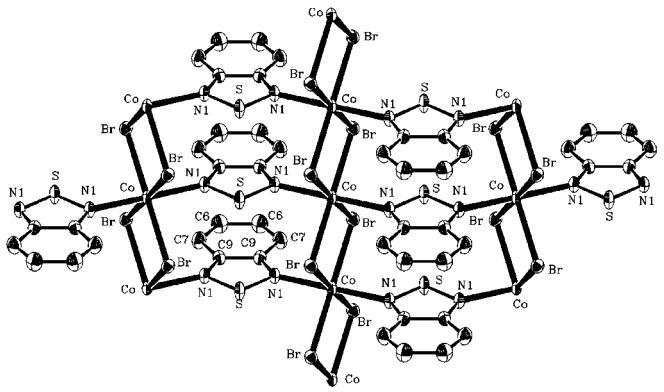

FIG. 1. Structure of **1** showing a single 2D layer (*ab* plane).

lattice, with the interplanar distances being 3.50 and 3.742 Å for free btd and **1**, respectively. In **1** the columns of the btd are orientated on alternating sides of each sheet. In addition to the van der Waals interactions, there are also short intralayer C ⋯ Br (C7 ⋯ Br, 3.616 Å, C7–H7 ⋯ Br = 126.1° and C7 ⋯ Br, 3.622 Å, C7–H7 ⋯ Br = 119.3°) and interlayer C ⋯ Br (C6 ⋯ Br, 3.955 Å, C6–H6 ⋯ Br = 148.0°) distances in **1**, possibly indicating weak C–H ⋯ Br hydrogen bonds (26, 27).

Reaction of btd with an equivalent of $CoCl_2$ in Me_2CO gives a green solution from which green microcrystalline $\{[CoCl_2(btd)]\}_n$ **2** precipitates within 1–2 min. in approx. 80% yield. Despite the fact that complex **2** is crystalline, we were unable to grow single crystals large enough for X-ray analysis. Complex **2** can also be isolated by employing $CoCl_2$:btd molar ratios of 2:1, 1:2, 1:3, 1:4, 1:5, and 1:6 in a variety of organic solvents like Me_2CO, MeCN, EtOH, Pr^nOH, and THF, as well as in several mixtures of these solvents.

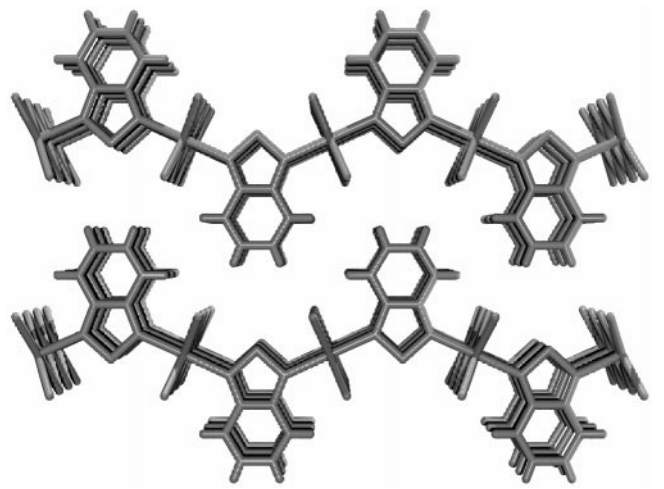

FIG. 2. Packing diagram of **1**, viewed approximately down *a*. Two layers are shown.

TABLE 4
Crystallographic Data for $\{[CoCl_2(btd)]\}_n$ (2)

Crystal system	Monoclinic
Space group	$P2_1/m$ (No. 11) [b unique]
a (Å)	3.575(28)
b (Å)	13.010(1)
c (Å)	8.798(68)
β (°)	91.997(2)
V (Å^3)	409(6)
Z	2
R_p[a]	0.1314
R_{wp}[b]	0.1848
R_F[c]	0.0579
R_{exp}[d]	0.0874

	Atomic coordinates			
	x	y	z	U_{iso} (Å^2)
Co	0.5	0.5	0	0.034(3)
Cl	0.009(2)	0.4466(4)	0.1715(6)	0.014(2)
N1	0.500	0.3463(3)	−0.100(1)	0.026(3)
S	0.500	0.25	0.0214(9)	0.026(3)[e]
C6	0.500	0.3052(3)	−0.514(1)	0.026(3)[e]
C7	0.500	0.3609(3)	−0.384(1)	0.026(3)[e]
C9	0.500	0.3061(3)	−0.244(1)	0.026(3)[e]

Note. In the following footnotes, $Y(i)_{obs}$, $F(i)_{obs}$, and $Y(i)_{calc}$, $F(i)_{calc}$ are the (observed and calculated) profile and structure factors, respectively, and w(i) is the statistical weight ($= 1/Y(i)_{obs}$).

[a] $R_p = \sum_i |Y(i)_{obs} - Y(i)_{calc}| / \sum_i Y(i)_{obs}$.

[b] $R_{wp} = \sum_i w(i)[Y(i)_{obs} - Y(i)_{calc}]^2 / \sum_i w(i) Y(i)^2_{obs}$.

[c] $R_F = \sum_i |F(i)_{obs} - F(i)_{calc}| / \sum_i F(i)_{obs}$.

[d] $R_{exp} = [(N - P) / \sum_i w(i) Y(i)^2_{obs}]^{1/2}$.

[e] Constrained to be equal to U_{iso} of N1.

The chloro complex (**2**) is isostructural with the bromo one (**1**), as revealed by XRD studies. The unit cell dimensions are given in Table 4. The Rietveld analysis diagrams are shown in Fig. 3. The structural model of **1** was used as a starting model for the Rietveld profile refinement with the program WinMPROF (28). A total of 514 reflections lie within the refined 2θ range. From the early stages of refinement it was realized that the Bragg peaks were anisotropically broadened and the best results were obtained by using the Anisotropic Variable Pearson VII function (29). Correction for peak asymmetry (30) was applied for peaks lying at angles lower than 15.0° (2θ value). The final values of fraction coordinates are listed in Table 4. The fractional coordinates of Cl were allowed to refine. Soft constrains were applied to bond distances and angles of the ligand molecule. The bonds N1–S, N1–C9, C9–C7, C7–C6, C9–C9*, and C6–C6* were constrained to the values 1.62(1), 1.36(1), 1.42(1), 1.35(1), 1.44(1), and 1.42(1) Å, respectively, and the angles C9–N1–S, N1–C9–C7, and C9–C7–C6 to the values 108.0(1), 127.4(1), and 117.5(1)°, respectively. The atoms C6* and C9* are derived from those given in Table 4 by applying the symmetry operation x, $-y + 0.5$, z. Usually all the atoms of the btd ligand lie on the same plane and this plane

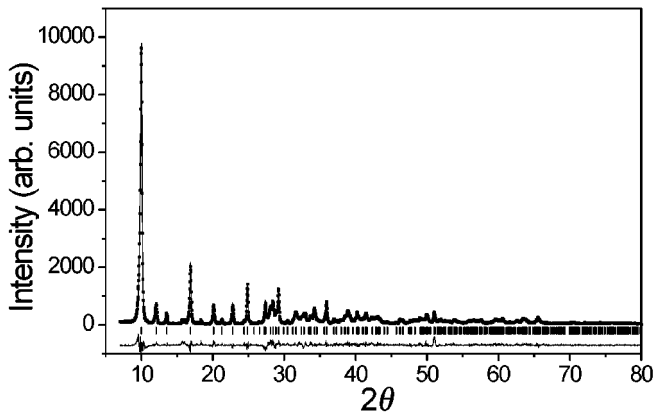

FIG. 3. XRD pattern of complex **2** refined by the Rietveld method. The filled bold squares are the experimental points. The continuous line corresponds to the calculated spectrum. Vertical bars (|) at the bottom indicate the position of the Bragg peaks. The continuous line at the bottom is the difference between the experimental intensity values and the calculated values.

is parallel to the (bc) crystallographic one; thus, the x coordinate for all the ligand atoms was constrained to the value of 0.5000.

The bond distances and angles for the ligand atoms lie within the constrained range. The Co–N1 bond distance is 2.188(4) Å, and the Co–Cl and Co–Cl′ (symmetry code for the Cl′ atom: $x + 1$, y, z) are 2.46(5) and 2.42(5) Å, respectively. The bond angle Cl–Co–Cl′ is 94.2°, and the angles Cl–Co–N1 and Cl′–Co–N1 are 90.0(2) and 88.8(2)°, respectively. The approach of the smaller Cl atoms (as they compare to the Br atoms) to the Co^{II} atoms has as a consequence of a slight increase of the Cl–Co–Cl′ angle and this is reflected in the β unit cell angle as well.

IR and UV/VIS Spectra

The FTIR spectra of complexes **1** and **2** are similar; they exhibit the typical bands of the disubstituted benzene ring and bands assignable to vibrations of the thiadiazole ring. The bands at approx. 1480 and 850 cm^{-1} are associated with the ν(CN) and ν(SN) vibrational modes of the thiadiazole ring (31), respectively. Due to coordination these bands are shifted compared to those in free btd.

Complexes **1** and **2** possess fairly similar solid-state electronic spectra (Table 5), in agreement with their similar structures. Both exhibit one halogen-to-cobalt(II) charge-transfer transition and d–d transitions at lower frequencies. The LMCT energy is lower in **1** than in **2** because the bromo ligand is more readily oxidizable than the chloro ligand (32). The d–d spectra can be assigned to transitions in high-spin d^7 octahedral (O_h) fields (32); the frequencies are typical of cobalt(II) chromophores rich in halogeno ligands. The multiple structure of the $^4T_{1g} \rightarrow {}^4T_{1g}$ (P) band arises primarily

TABLE 5
Solid-State Electronic Spectral Data for Complexes 1 and 2

Assignment[a]/parameter	1	2
LMCT (10^3 cm^{-1})	25.64	27.03
$^4T_{1g} \rightarrow {}^4T_{1g}$ (P) (10^3 cm^{-1})	17.86, 16.39	19.02, 17.33
$^4T_{1g} \rightarrow {}^4A_{2g}$ (10^3 cm^{-1})	13.79 sh	14.37 sh
Calcd. $^4T_{1g} \rightarrow {}^4T_{2g}$ (10^3 cm^{-1})[b]	6.42	6.69
$10D_q$ (cm^{-1})[b]	740	770
B (cm^{-1})[b]	777	832
β[c]	0.80	0.86

Note. B = Racah parameter; LMCT = ligand-to-metal charge-transfer; sh = shoulder.

[a] Assignments are given, assuming a ligand field of O_h symmetry.

[b] Calculated as described in Appendix V of Ref. (32).

[c] B (free ion) = 971 cm^{-1}.

from the admixture of spin-forbidden transitions to doublet states mainly derived from ^2G and ^2H (32). The transition to $^4A_{2g}$ is very weak as expected (32), appearing as a shoulder.

Magnetic Properties and Theoretical Calculations

The two compounds show similar magnetic properties (Fig. 4) as may be expected from the similar structural topology. On cooling, the $\chi_M T$ product of both complexes decreases continuously, tending to 0 at 2 K. The susceptibility plot shows a continuous increase when T decreases up to a maximum placed at 3.5 K for **1** and 5.5 K for **2**. Below these temperatures the χ_M values decrease, reaching values close to those expected for a 2D system. This behavior indicates an overall weak antiferromagnetic coupling. Measurements performed under different external fields (between 300 and 10,000 G) show that the magnetic susceptibility is independent of the field and, thus, long-range order phenomena are not present. Evaluation of the coupling constants is not possible for both compounds due to the

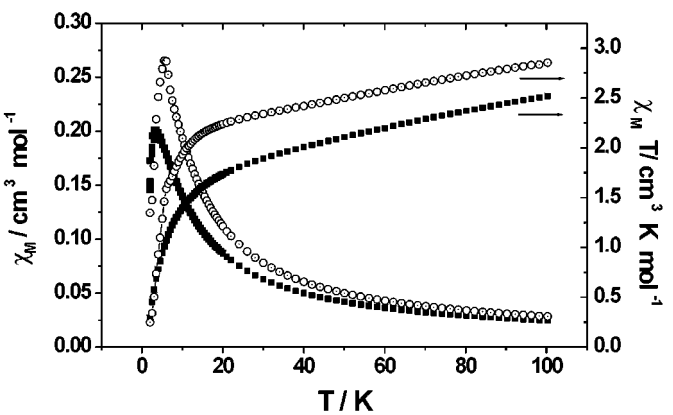

FIG. 4. Plots of $\chi_M T$ and χ_M vs T for complexes **1** (filled squares) and **2** (dot-centered circles).

large anisotropy of the Co^{II} ions and to the alternating 2D topology of the system, for which analytical expressions are not available.

The X-band EPR spectra of **1** and **2**, recorded on powdered samples at 4 K, are practically identical (Fig. 5), showing an intense signal around $g = 4$ and weaker signals in the $g = 2$ region. These spectra correspond to typical axially distorted $S = \frac{3}{2}$ systems in good agreement with structural data.

Despite the fact that quantitative analysis of the magnetic data is not possible, the interaction pattern may be deduced from the above magnetic data and by comparison with other related systems. The coupling along the chains defined by the dihalide bridges, with Co–X–Co bond angles slightly greater than 90°, should be ferromagnetic as it has been pointed out for the reported polymeric $CoCl_2 \cdot 2H_2O$, $CoCl_2(py)_2$ [py = pyridine] and CoX_2(4,4′-bpy) [4,4′-bpy = 4,4′-bipyridine] complexes (18).

To determine the origin of the AF dominant coupling, MO analysis (33) of the interaction pathway provided by the btd ligand has been performed on a fragment modeled as a dinuclear unit $[(NH_3)_5\text{–Co–btd–Co}(NH_3)_5]^{4+}$. In this model the Co–$NH_3$ bond distances were fixed at 2.100 Å, whereas the experimental bond distances and angles provided by the structural data of **1** have been used in the (Co–btd–Co) bridging region. The MO results have been analyzed according to the Hoffmann model (34), which relates the magnitude of the AF interaction with the square of the gap between pairs of molecular orbitals with the same symmetry. The MO's diagram indicates that the t_{2g} and one of the e_g symmetry combinations of the atomic orbitals of the Co^{II} ions do not contribute to the coupling, due to the poor overlap with the π system of the bridging ring. In contrast, the d_{z^2} atomic orbitals of the Co^{II} ions overlap with one of the empty σ molecular orbitals of the btd bridge, showing a gap between the symmetric and antisymmetric

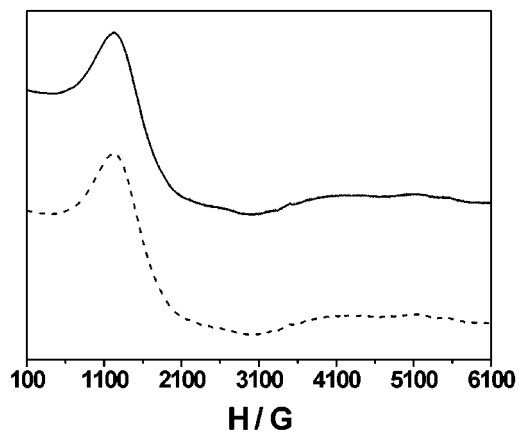

FIG. 5. X-band powder EPR spectra of complexes **1** (solid line) and **2** (dashed line) at 4 K.

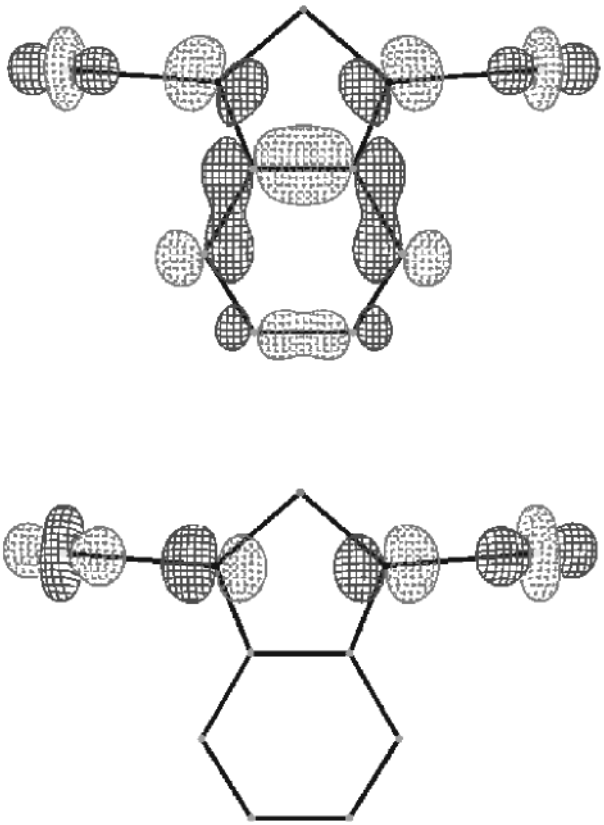

SCHEME 1.

antibonding MOs of $\Delta = 0.24$ eV, which is coherent with moderate antiferromagnetic interaction (Scheme 1). A moderate AF magnetic interaction has been reported for a tetranuclear copper(II) cation that consists of two $Cu_2(\mu\text{-Im})^{3+}$ units (Im = imidazolate ion) [35].

Overall, compounds **1** and **2** may be magnetically described as moderately AF $(Co\text{–btd–Co})_\infty$ chains with $S = 0$ ground state. The weaker ferromagnetic interactions, promoted by the dihalide bridges between the $(Co\text{–btd–Co})_\infty$ chains, may modulate the shape of the $\chi_M T$ or χ_M vs T plots, but they do not affect the $S = 0$ ground state (Fig. 6). This description of the interaction pattern does not indicate any metamagnetic low-temperature behavior.

CONCLUSIONS

One of the main challenges in crystal engineering is to carry over robust modules or motifs from the crystal of one compound to that of another. This work reports the structural, spectroscopic, and magnetic characterization of two 2D coordination polymers based on the planar organic ligand 2,1,3-benzothiadiazole (btd), and cobalt(II) chloride and bromide. The columns of stacked btd molecules present in the crystal structure of the free ligand are maintained in

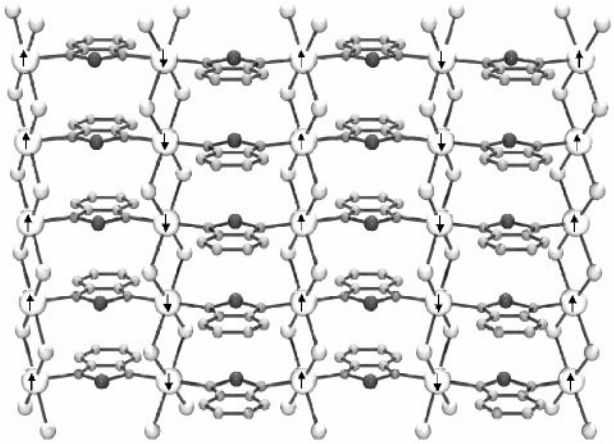

FIG. 6. The interaction pattern for complexes **1** and **2**.

the 2D lattices of **1** and **2**. In other words, a strong (but not exclusive) driving force for the construction of the lattices of btd and its complexes is the π–π interactions between the btd molecules. It seems that the rigid columns of stacked ligand molecules serve as "macroscopic" templates on which the CoX_2 units are assembled in such a way that the resulting structures preserve the directionality of the intermolecular interaction; this conclusion is strengthened by our recent single-crystal, X-ray structural determinations of the 2D complexes $\{[CuCl(btd)]\}_n$ and $\{[CuCl_2(btd)]\}_n$. The purely chemical message of this work is the idea that the coordination bonds and aromatic stacking interactions can be forged into a supramolecular tool that has not yet been employed in a systematic manner.

The magnetic properties observed in **1** and **2** are attributed to the very weak ferromagnetic intrachain Co···Co exchange interaction through the $(\mu\text{-}X)_2$ bridges ($X = Cl$, Br) along the *a* axis and the moderate antiferromagnetic intrachain Co···Co interaction through the μ-btd bridges along the *b* axis. Recently Li and coworkers (18) reported the 2D coordination polymer $\{[CoCl_2(4,4'\text{-bpy})]\}_n$, which has a structure rather similar to that of **1** and **2**. A spontaneous antiferromagnetic ordering was found from the χ_M vs T measurements under low fields with a transition temperature of 5.0 K. The χ_M vs T (under different fields) and the magnetization (M) vs H (at 2 K) data exhibited a metamagnetic behavior in that the ground-state magnetic structure changes upon the change in the applied field. Below a critical field, H_c, the ground-state magnetic structure is antiferromagnetic; when the applied field is stronger than H_c, the ground state is ferromagnetic-like or paramagnetic-like (18). The magnetic difference between **1** and **2** and $\{[CoCl_2(4,4'\text{-bpy})]\}_n$ is due to the fact that the Co···Co distance through the μ-4,4′-bpy bridge is too long (approx. 11.5 Å) for any significant magnetic interaction; in fact, this interaction is very weakly antiferromagnetic and the 4,4′-bpy complex is a 2D coordination polymer with 1D $(Co\text{–}Cl_2\text{–}Co)_\infty$ magnetic chains. In contrast, in **1** and **2** the moderate antiferromagnetic interaction through the μ-btd bridges predominates over the very weak ferromagnetic interaction through the $(\mu\text{-}X)_2$ bridges and this does not lead to any metamagnetic low-temperature behavior.

Efforts are in progress to replace the X^- bridging ligands in **1** and **2** with other monoatomic bridges, e.g., end-on (EO) azides (N_3^-), that lead to stronger ferromagnetic coupling, with the hope of isolating molecular ferromagnets.

ACKNOWLEDGMENT

The authors gratefully acknowledge the Greek General Secretariat of Research and Technology (Grant 99ED139 to V.P.) for support of this work.

REFERENCES

1. R. Robson, B. F. Abrahams, S. R. Batten, R. W. Gable, B. F. Hoskins, and J. Liu, "Supramolecular Architecture," Chap. 19. *Am. Chem. Soc.*, Washington, DC, 1992.
2. G. R. Desiraju, *Angew. Chem. Int. Ed. Engl.* **34,** 2311 (1995).
3. D. Braga, F. Grepioni, and A. G. Orpen (Eds.), "Crystal Engineering: From Molecules and Crystals to Materials," NATO Science Series, Series C, Vol. 538, Kluwer Academic, Dordrecht, 1999.
4. K. N. Power, T. L. Hennigar, and M. J. Zaworotko, *New J. Chem.* 177 (1998).
5. M. O'Keeffe, M. Eddaoudi, H. Li, T. Reineke, and O. M. Yaghi, *J. Solid State Chem.* **153,** 3 (2000), doi:10.1006/jssc.2000.8723.
6. C. B. Aakeröy, A. M. Beatty, and D. S. Leinen, *Angew. Chem. Int. Ed.* **38,** 1815 (1999).
7. C. B. Aakeröy, A. M. Beatty, D. S. Leinen, and K. R. Lorimer, *Chem. Commun.* 935 (2000).
8. G. Guilera and J. W. Steed, *Chem. Commun.* 1563 (1999).
9. C. A. Hunter, *Chem. Soc. Rev.* 101 (1994).
10. L. R. MacGillivray, R. H. Groeneman, and J. Atwood, *J. Am. Chem. Soc.* **120,** 2676 (1998).
11. V. Luzzati, *Acta Crystallogr.* **4,** 193 (1951).
12. M. Munakata, T. Kuroda-Sowa, M. Maekawa, M. Nakamura, S. Akiyama, and S. Kitagawa, *Inorg. Chem.* **33,** 1284 (1994).
13. M. W. Renner, K. M. Barkigia, D. Melamed, K. M. Smith, and J. Fajer, *Inorg. Chem.* **35,** 5120 (1996).
14. A. F. Hill and J. D. E. T. Wilton-Ely, *J. Chem. Soc. Dalton Trans.* 3501 (1998).
15. W. Kaim and S. Kohlman, *Inorg. Chim. Acta* **101,** L21 (1985).
16. T. Sekine, T. Okuno, and K. Awaga, *Inorg. Chem.* **37,** 2129 (1998), and references therein.
17. F. Lloret, G. De Munno, M. Julve, J. Cano, R. Ruiz, and A. Caneschi, *Angew. Chem. Int. Ed.* **37,** 135 (1998).
18. M. A. Lawandy, X. Huang, R.-J. Wang, J. Li, J. Y. Lu, T. Yuen, and C. L. Lin, *Inorg. Chem.* **38,** 5410 (1999).
19. M. Kurmoo, *Phil. Trans. R. Soc. London A* **357,** 3041 (1999).
20. G. De Munno, T. Poerio, G. Viau, M. Julve, F. Lloret, Y. Journaux, and E. Riviére, *Chem. Commun.* 2587 (1996).
21. S. O. H. Gutschke, D. J. Price, A. K. Powell, and P. T. Wood, *Angew. Chem. Int. Ed.* **38**, 1088 (1999).
22. E. Coronado, J. R. Galán-Mascarós, C. J. Gómez-Carcía, J. Ensling, and P. Gütlich, *Chem. Eur. J.* **6,** 552 (2000).
23. G. M. Sheldrick, "SHELXS-86, Structure Solving Program." University of Gottingen, Germany (1986).

24. G. M. Sheldrick, "SHELXL-93, Crystal Structure Refinement." University of Gottingen, Germany (1986).
25. J. Pickardt and B. Staub, *Z. Naturforsh. B* **52,** 1456 (1997).
26. R. Kuhlman, G. L. Schimek, and J. W. Kolis, *Polyhedron* **18,** 1379 (1999).
27. D. Braga, S. M. Draper, E. Champeil, and F. Grepioni, *J. Organomet. Chem.* **573,** 73 (1999).
28. "WinMprof: A Visual Rietweld Software," *CPD News Letter* **21,** 13 (1999).
29. A. Le Bail and A. Jouanneaux, *J. Appl. Crystallogr.* **30,** 265 (1997).
30. J. F. Berar and G. Baldinozzi, *J. Appl. Crystallogr.* **26,** 128 (1993).
31. A. A. El-Azhary, *Spectrochim. Acta A* **52,** 33 (1996).
32. A. B. P. Lever, "Inorganic Electronic Spectroscopy," 2nd ed. Elsevier, Amsterdam, 1984.
33. C. Mealli and D. M. Proserpio, "CACAO, Computed Aided Composition of Atomic Orbitals, Version 4.0," *J. Chem. Educ.* **67,** 3399 (1990).
34. J. P. Hay, J. C. Thibeault, and R. Hoffmann, *J. Am. Chem. Soc.* **97,** 4884 (1975).
35. H.-L. Zhu, L.-M. Zheng, D.-G. Fu, P. Huang, W.-M. Bu, and W.-X. Tang, *Inorg. Chim. Acta* **287,** 52 (1999).